Earth and Planetary Science Letters 584 (2022) 117418

Contents lists available at ScienceDirect

Earth and Planetary Science Letters

www.elsevier.com/locate/epsl

Flame out! End-Triassic mass extinction polycyclic aromatic hydrocarbons reflect more than just fire

C.P. Fox [a,*,1], J.H. Whiteside [b], P.E. Olsen [c], K. Grice [a]

[a] Western Australia Organic & Isotope Geochemistry Centre, School of Earth and Planetary Sciences, The Institute for Geoscience Research, Curtin University, Perth, Western Australia 6845, Australia
[b] Ocean and Earth Science, National Oceanography Centre Southampton, University of Southampton, Southampton SO14 3ZH, United Kingdom
[c] Department of Earth and Environmental Sciences, Lamont-Doherty Earth Observatory of Columbia University, 61 Route 9W, Palisades, NY 10964, USA

ARTICLE INFO

Article history:
Received 13 August 2021
Received in revised form 24 January 2022
Accepted 6 February 2022
Available online 18 March 2022
Editor: B. Wing

Keywords:
end-Triassic mass extinction
St. Audrie's Bay
PAHs
biomarkers
organic geochemistry

ABSTRACT

Global warming induced-wildfires of the 21st century reveal the catastrophic effects that widespread biomass burning has on flora and fauna. During mass extinction events, similar wildfire episodes are considered to play an important role in driving perturbations in terrestrial ecosystems. To better evaluate the record of biomass burning and potential carbon cycle feedbacks at the end-Triassic mass extinction (~202 Ma; ETE), we investigated the relative abundances of a range of polycyclic aromatic hydrocarbons (PAHs) and the $\delta^{13}C$ values of regular isoprenoids and *n*-alkanes at key sections in the SW UK. These data reveal little evidence for intensive wildfire activity during the extinction event, in contrast to what has been reported elsewhere in European, Chinese, and Greenland ETE sections. Herein, PAHs instead reflect greater contributions from an episode of soil erosion that we attribute to Large Igneous Province (LIP)-driven acid rain, and possible distal sources of smoke, suggestive of fire elsewhere in the UK/European basins. This terrestrial ecosystem perturbation is coincident with those in the marine realm, indicating ecosystem perturbations occurred across multiple habitats throughout the latest Rhaetian in the SW UK. Additionally, this geochemical approach reveals that the precursor carbon isotope excursion (CIE) routinely used in chemostratigraphic correlations is unrelated to LIP activity, but instead results from the increased input of terrestrially derived ^{13}C-depleted plant material. Furthermore, we find the initial CIE (commonly used to mark the extinction level, but which is now known to precede the ETE) is also unrelated to biomass burning. Collectively, these data reveal that processes other than combustion of terrestrial material are important for the terrestrial phase of the ETE in the SW UK. Similar investigations are required on other ETE sections, both those in close proximity to the LIP driving the extinction and those further afield, to more clearly determine the negative effect(s) of LIPs and their geographic extent in the terrestrial realm.

1. Introduction

The climate change-driven increases in the frequency and intensity of forest fires in the last decade illustrate the lethal effects fire events have on terrestrial ecosystems. For example, more than one billion vertebrates are estimated to have died during the 2019/2020 Australian bushfires (Dickman and McDonald, 2020). Similar events, although from deep time records, are thought to have been important for driving terrestrial ecosystem perturbations during mass extinction events, including the end-Triassic mass extinction event (ETE) at ~201.5 Ma (Wotzlaw et al., 2014). Propelling this extinction event was the emplacement of Earth's most laterally extensive large igneous province (LIP), the Central Atlantic Magmatic Province (CAMP), triggering a series of cascading environmental effects that proved catastrophic for end-Triassic life: anoxia, euxinia, acidification, global warming driven by CO_2 increases, mercury and other volatile emissions, eutrophication, lithospheric bulging/collapse resulting in sea-level change, and a possible short-lived SO_2-induced intense cooling that may also have affected sea-level (e.g., Pálfy, 2003). Similar to the wildfire events of the last decade, widespread and intense CAMP-induced wildfires are expected to have had major impacts on terrestrial life, particularly for regions in close proximity to the CAMP. However, the extent, duration, intensity, and synchronicity of such events remains unclear.

* Corresponding author.
E-mail address: Calum.Fox@ku.ac.ae (C.P. Fox).
[1] Current address: Khalifa University of Science and Technology, PO Box 127788, Abu Dhabi, UAE.

https://doi.org/10.1016/j.epsl.2022.117418
0012-821X/

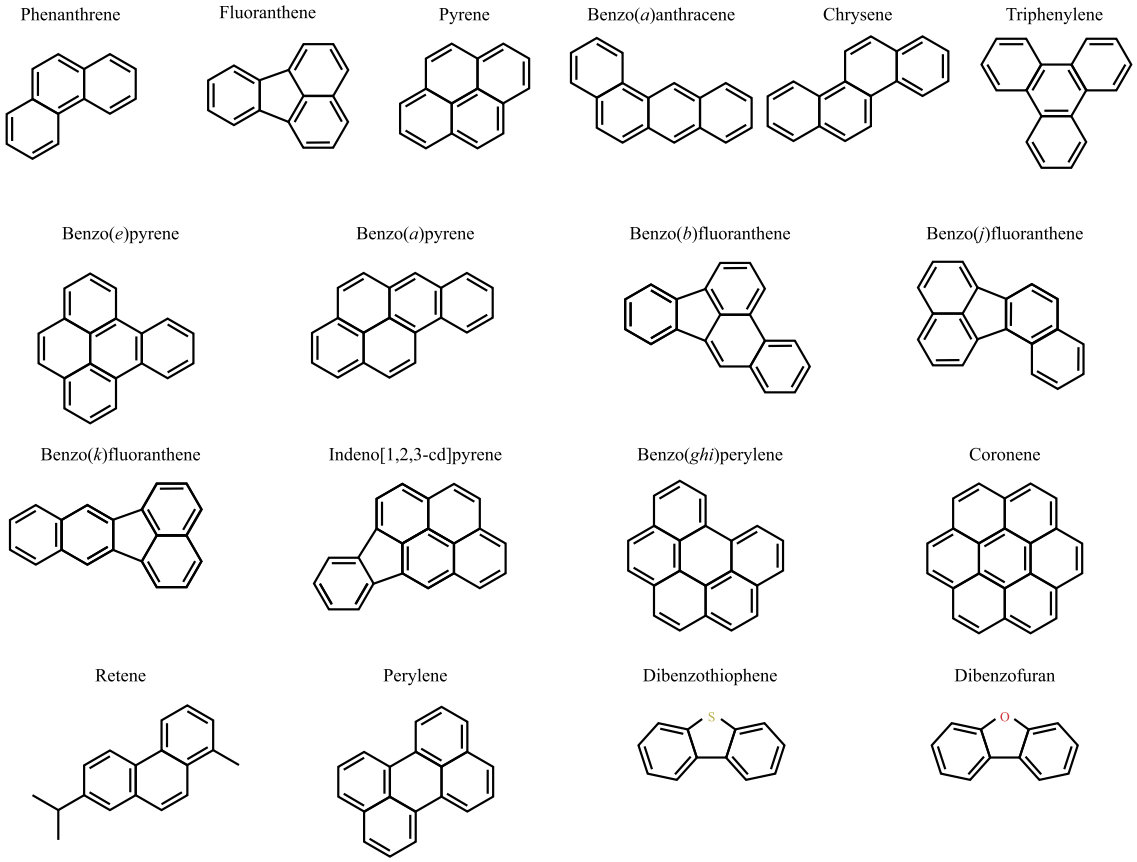

Fig. 1. Polycyclic Aromatic Hydrocarbon (PAH) structures discussed in this study. Note that benzo(*bjk*)fluoranthene here is separated into the individual compounds benzo(*b*)fluoranthene, benzo(*j*)fluoranthene, benzo(*k*)fluoranthene. For further details see Table 1.

Table 1
Abbreviations of PAH compounds and information on methyl and ethyl groups used in figures 6 and 7. Ring numbers of each PAH compound given in parentheses.

Compound and ring no.	Abbreviation	Methyl/Ethyl Compound no.	Compound and ring no.	Abbreviation	Methyl/Ethyl Compound no.
Dibenzothiophene (3)	DBT	-	Benzo(*a*)anthracene (4)	BaA	-
Dibenzofuran (3)	DBF	-	Chrysene & Triphenylene (4)	C&T	-
Methyldibenzofurans (3)	DBF1	all	Benzo(*e*)pyrene (5)	BeP	-
Fluorene (3)	F	-	Benzo(*a*)pyrene (5)	BaP	-
Anthracene (3)	A	-	Benzo(*bjk*)fluoranthene (5)	BbjkF	-
Phenanthrene (3)	P	-	Indeno[1,2,3-cd]pyrene (6)	IP	-
Methylphenanthrenes (3)	P1	1- and 2-	Benzo(*ghi*)perylene (6)	BghiP	-
Ethylphenanthrenes (3)	P2	1-,2-, and 9-	Coronene (7)	Cor	-
Fluoranthene (4)	FL	-	Perylene (5)	PER	-
Methylfluoranthenes (4)	FL1	-	Retene (3)	RET	-
Pyrene (4)	PY	all			
Methylpyrenes (4)	PY1	all			

In addition to charcoal, a proxy for investigating wildfire activity in the geological record is the abundances of Polycyclic Aromatic Hydrocarbons (PAHs) that can be important indicators of organic matter formed at higher temperatures, such as those associated with incomplete combustion during wildfires. Combustion-derived PAHs (pyPAHs) typically used to investigate periods of paleowildfire activity include phenanthrene, fluoranthene, pyrene, benzo(*a*)anthracene, chrysene, triphenylene, benzo(*e*)pyrene, benzo(*a*)pyrene, benzo(*bjk*)fluoranthene, Indeno[1,2,3-cd]pyrene, benzo(*ghi*)perylene, and coronene (Fig. 1; Table 1), with those having a high-molecular-weight (HMW; i.e., compounds containing five or more aromatic rings) best representing evidence of paleowildfires. However, PAHs can originate from a wide range of sources other than just combustion (i.e. wildfires); these include volcanism, hydrothermal fluids and the diagenesis/catagenesis of biogenic precursors (see Holman and Grice, 2018). Additionally, pyPAH ratios can serve as proxies beyond paleowildfires, e.g., helping to infer organic matter origin (Denis et al., 2021) or reflect changes in the hydrological cycle (Finkelstein et al., 2005). Furthermore, low-molecular-weight (LMW) PAHs (Fig. 1) can arise from increased weathering and soil erosion (Fenton et al., 2007; Sephton et al., 2005). Thus far, PAH distributions in European, East Greenland and Chinese ETE and early Jurassic sections have been attributed to the CAMP-induced combustion processes (Fang et al., 2021; Marynowski and Simoneit, 2009; Song et al., 2020; van de Schootbrugge et al., 2009; Williford et al., 2014; Zhang et al., 2020) (Fig. 2). However, some of these studies lack more recent but critical findings such as determining whether pyPAHs are of petrogenic (oil/coal-related) or pyrogenic (fire-related)

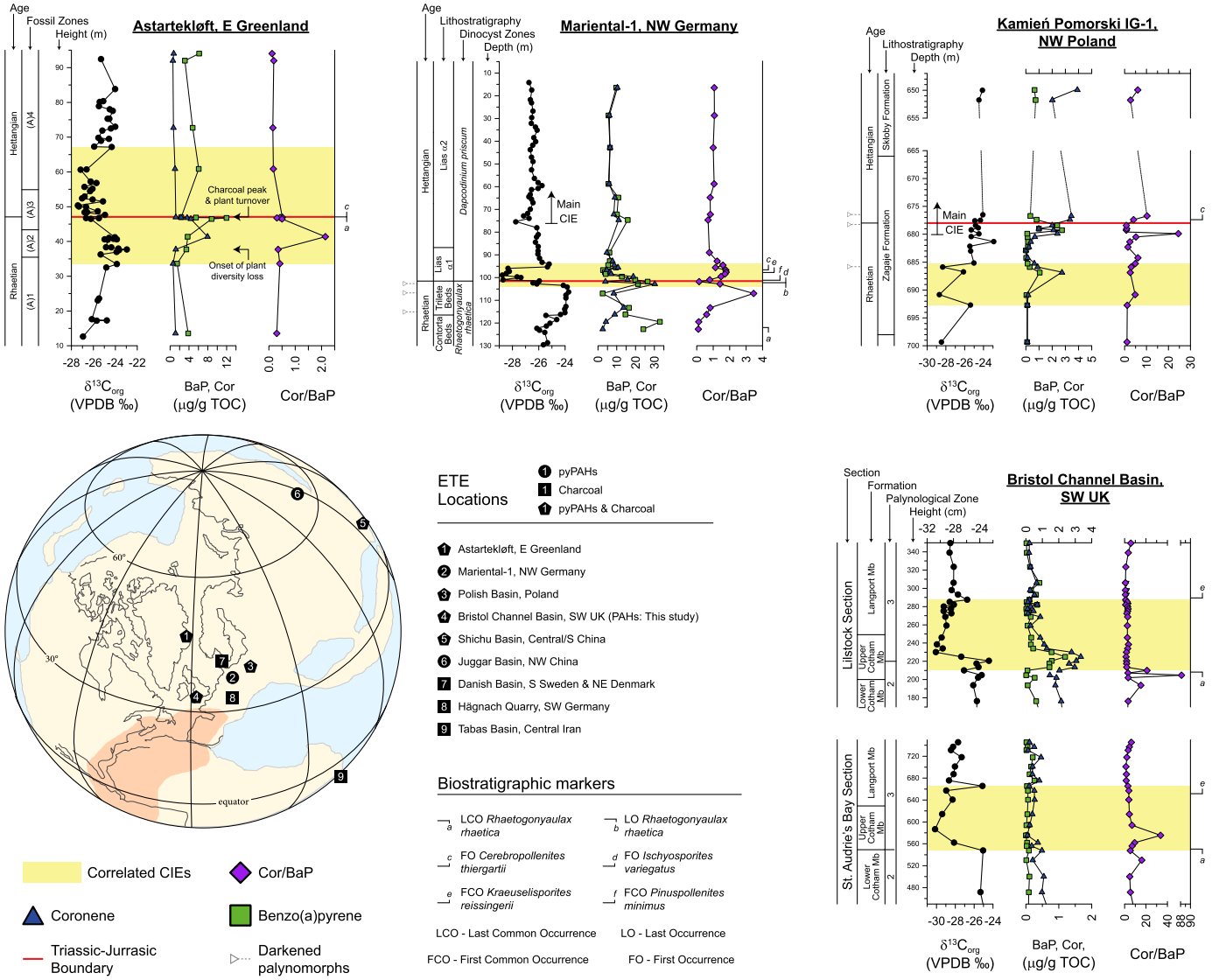

Fig. 2. pyPAHs and charcoal during the ETE. Bottom left: reconstruction of the ETE with lateral extent of the CAMP (in red) and approximate geographic locations of charcoal bearing units and pyPAH studies (key given in figure) (Alipour et al., 2021; Belcher et al., 2010; Fang et al., 2021; Harris, 1958; Petersen and Lindström, 2012; Pole et al., 2018; Song et al., 2020; Uhl and Montenari, 2011; van de Schootbrugge et al., 2009; Williford et al., 2014; Zhang et al., 2020). Full pyPAH profiles for locations 1-4 expressed relative to the $\delta^{13}C_{org}$ record with correlated CIEs given in the highlighted areas. Astartekløft (1) $\delta^{13}C_{wood}$ profile from Hesselbo et al. (2002), PAH abundances from Williford et al. (2014), charcoal evidence from Belcher et al. (2010), sporomorph/macrofossil ecological zones after Mander et al. (2013), and plant diversity loss/turnover from McElwain et al. (2009 and refs therein). Mariental-1 (2) $\delta^{13}C_{org}$ record after van de Schootbrugge et al. (2013), PAH abundances and dinocyst zones from van de Schootbrugge et al. (2009), and biostratigraphy after Heunisch et al. (2010). Kamień Pomorski IG-1 (3) $\delta^{13}C_{org}$ record and biostratigraphy after (Pieńkowski et al., 2011), PAH abundances from (Marynowski and Simoneit, 2009). SW UK (4) $\delta^{13}C_{org}$ reconstructions from Fox et al. (2020), PAH abundances from this study, and palynological zones after (Bonis et al., 2010). Key for PAH compounds and biostratigraphic markers given next to ETE reconstruction. Biostratigraphic markers used follow those used in correlations of Lindström et al. (2017). Plot abbreviations: Cor/BaP – Coronene/Benzo(a)pyrene; TOC – Total Organic Carbon; VPDB – Vienna Pee Dee Belemnite. (For interpretation of the colours in the figure(s), the reader is referred to the web version of this article.)

origins and if pyPAHs represent smoke or residue sources (Karp et al., 2020).

Linking the CAMP-induced environmental perturbations, including paleowildife events, among globally dispersed localities has mostly relied on chemostratigraphic correlations using carbon isotope excursions (CIEs) in the bulk organic carbon isotope ($\delta^{13}C_{org}$) record. The ETE contains three, often distinct, CIEs typically termed the precursor CIE (or Marshi CIE), the initial CIE (or Spelae CIE), and the main CIE (or top-Tilmanni CIE), as observed in European (Tethys/Pangea), North American and Japanese (Panthalassic Ocean) Triassic-Jurassic boundary sections (e.g. Lindström et al., 2017). Increases in ETE pyPAHs in sections from Greenland, Poland, Germany, and China, coincide with shifts in palynomorphs and occur at or close to CIEs used in these chemostratigraphic correlations (Fang et al., 2021; Marynowski and Simoneit, 2009; Song et al., 2020; van de Schootbrugge et al., 2009; Williford et al., 2014; Zhang et al., 2020) (Fig. 2). The precursor, initial, and main CIEs are used as chemostratigraphic markers since they are hypothesized to express the CAMP-induced release of isotopically light (^{12}C) methane clathrates (Hesselbo et al., 2002) and/or thermogenic carbon (Davies et al., 2017) into the global ocean–atmosphere system. However, in the SW UK, typically considered an ETE type locality and the site to which almost all other ETE $\delta^{13}C_{org}$ records are compared, the initial CIE seems better explained as being driven by the emergence of shallow-water microbial mats, amongst other dramatic ecological and environmental changes associated with sea-level change (Beith et al., 2021; Fox et al., 2020). Additionally, the succeeding main CIE instead reflects the shift to prolonged negative $\delta^{13}C_{org}$ values associated with the extinction, spanning the Hettangian and early Sinemurian (Fox et al., 2020). Similar inves-

tigations to determine the origin of the precursor CIE have not yet been presented, hindering the robustness of chemostratigraphic correlations using this CIE.

Currently, there is a lack of understanding relating to the timing, duration, and global extent of ETE paleowildfires and the validity of the precursor CIEs as a chemostratigraphic marker. To better understand these processes during the ETE, as well as other mass extinction events and intervals of biotic crises, this study aims to 1) evaluate terrestrial biomass burning as the major source of end-Triassic PAHs and help determine whether CAMP-induced biomass burning occurred at a global scale; and 2) probe the robustness of the precursor CIE in relation to the CAMP and chemostratigraphic correlations. To answer these questions, we undertook a high-resolution (i.e., at cm sampling intervals) study of PAH distributions and $\delta^{13}C$ values of *n*-alkanes and regular isoprenoids originating from lower trophic organisms (phytoplankton/ bacteria) and higher plants at two neighbouring ETE sections in the Bristol Channel Basin, UK (St. Audrie's Bay and Lilstock).

2. Studied sections

The Bristol Channel Basin, SW UK that includes the St. Audrie's Bay (51.182833°, -3.286000°) and Lilstock (51.200757°, -3.176389°) sections, is well characterized in terms of paleontology, palynology, and geochemistry (see supplementary information for full details). Importantly, the St. Audrie's Bay is a focal ETE section to which many records are compared, hence, the selection of these study sites. The late Rhaetian to early Hettangian age strata (Triassic-Jurassic boundary transition) are represented by the Westbury, Lilstock, and Blue Lias formations, with the Lilstock Formation subdivided into the Cotham and Langport members. Here we briefly describe these depositional settings, for full details see the supplementary information.

The Westbury Formation, a regionally extensive marine unit that contains the precursor CIE, consists of dark grey to black organic rich mudstones ("shales") and subordinate silty calcareous mudstones that are interbedded with grey limestone concretions. The Formation generally represents a calm offshore but shallow sea with maximum flooding surface in the middle of the Formation, possibly below the precursor CIE recorded in the middle/upper portion of the Formation (Hesselbo et al., 2004).

Overlaying the Westbury Formation, the Cotham Member contains green-grey calcareous mudstones, subordinate limestones, sandstones, and evidence of seismites. Soft sediment deformation of sandstones that are cut by siltstone-filled desiccation cracks (above which a hiatus is recorded), wave ripples, and possible raindrop imprints indicate a shallower water environment. The Cotham Member is separated into the upper and lower units above and below where the first (and deepest) desiccation cracks occur, at which point the initial CIE begins. Water depth is inferred to shallow upward through the lower Cotham Member, although marine pelagophytes swiftly reduce at the boundary between the Westbury Formation and Cotham Member suggesting a regression event (Fox et al., 2020; Hesselbo et al., 2004). This interval, especially the upper part, is marked by a near absence of marine biota, representing a shallow brackish to freshwater lagoon-type environment, on the order of 10s of cm at some intervals (Fox et al., 2020 and refs therein; Mander et al., 2008; Wignall and Bond, 2008 and refs therein).

The Langport Member contains nodular/laminated peloidal and microspar pale grey limestones with marine fossils returning in close proximity to a minor transgression event and termination of the initial CIE (Fox et al., 2020; Mander et al., 2008; Wignall and Bond, 2008). In the SW UK, this Member has been described as representing the distal part of a carbonate ramp (Hesselbo et al., 2004), or a warm, shallow, carbonate-rich lagoon (Hounslow et al., 2004) punctuating more humid conditions with increased aridity (Wignall and Bond, 2008). Biomarkers of microbial mat containing organisms, laminar and thrombolytic stromatolites, and an absence of metazoans are evidenced within the Cotham and Langport members during the initial CIE supporting the formation of microbial mats that likely accounts for the initial CIE (Fox et al., 2020 and refs therein). The initial CIE and apparent "dead zone" is purported to mark the extinction horizon (Mander et al., 2008). However, lack of marine biota at this interval is simply explained by low water depth and low salinity.

The transition from the Langport Member to the Blue Lias Formation is marked by a flooding event, in which marine water quickly became stratified, anoxic, euxinic and acidic (Fox et al., 2022), resulting in deposition of organic-matter rich, highly lithified black shales, termed the paper shales. Better placement for the extinction horizon is within the very basal Blue Lias Formation coincident with a Lilliput assemblage of bivalves, last occurrences of conodonts and the reptile clade Phytosauria (Fox et al., 2020; Wignall and Atkinson, 2020), as well as the strongest evidence of CAMP-driven environmental perturbations (Beith et al., 2021 and refs therein; Fox et al., 2022). The water depth during deposition of this portion of the Blue Lias Formation was at least 10s of meters thick preventing influence of wave action on bottom waters.

In this study, samples from St. Audrie's Bay span the upper two meters of the Westbury Formation, through Cotham and Langport members to the very base of the Blue Lias Formation and samples from Lilstock begin at the very top of the Westbury Formation, continue through the Cotham and Langport members, and the lower 1.2 m of the Blue Lias Formation.

3. Analytical methods

3.1. Sample preparation, separation, Gas Chromatography-Mass Spectrometry (GC-MS) and GC-Isotope Ratio Mass Spectrometry (GC-IRMS) analysis

Sediment/rock samples weighing more than ~100 g were collected at ~10 cm intervals using a rock hammer from outcrops at St. Audrie's Bay (55 samples) and Lilstock (60 samples). Surface edges of samples were removed (~5 cm of all edges of non-shale samples) and samples were sonicated in 9:1 dichloromethane:methanol (DCM:MeOH; 15 min, 3 times) to remove any surface organic matter contamination. Samples were crushed using a Rocklabs SRM C+PB rock grinder. Between 30-180 g of rock was extracted using a Milestone Start-E microwave extraction system in 50 mL of 9:1 DCM:MeOH using a temperature program of 21 °C to 80 °C over 10 min (held at 80 °C for 15 min). Samples rich in extractable organic material (TOC >2%) were re-extracted to ensure all organics had been collected. Copper turnings were solvent washed (15 min, sonicated in 9:1 DCM:MeOH) and activated (30 min in 2M hydrochloric acid; HCl) and added to samples to remove elemental sulphur. Samples were then fractionated into saturate (*n*-hexane), aromatic (9:1 *n*-hexane:DCM) and polar (9:1 DCM:MeOH) fractions using activated silica gel (heated to 160 °C overnight) using columns varying from 4 cm Pasteur pipettes (7.5 g silica gel) to 20 cm x 1.5 cm glass columns (40 g silica gel). An internal standard (deuterated phenanthrene; 300 or 600 ng) was added to the aromatic fraction to quantify PAHs.

The PAH-containing aromatic fractions were analyzed using an Agilent 6890N GC with splitless injection and DB-5MS (60 m length, 0.25 mm diameter, 0.25 µm film thickness) capillary column coupled to an Agilent 5975B MS. The GC temperature program was 3 °C/min from a 40 °C initial start temperature to 325 °C, where temperature was held (30 min). Helium was used as the carrier gas (constant flow rate 1.1 mL/min). Samples were run using selected ion monitoring (SIM) analysis (see Supplementary In-

formation Table S1) for all PAHs of interest (Table 1). These PAHs include a wide range of LMW and HMW compounds typically used to investigate past wildfire events (see Karp et al., 2020) or other processes associated with mass extinction events, such as soil erosion (e.g., Fenton et al., 2007). PAH compounds were identified by comparing retention times, elution patterns, and extracted ions to standards (Neochema PAH mix) and PAHs reported in the literature. All glassware was combusted overnight (at 550 °C) and all materials were washed in 9:1 DCM:MeOH to remove contamination.

The *n*-alkane-containing saturate fractions were first analyzed using an Agilent 6890 GC with splitless injection and DB-1MS (60 m length, 0.25 mm diameter, 0.25 μm film thickness) capillary column connected to an Agilent 5973 MS. The GC program was 3 °C/min from a 40 °C initial start temperature to 325 °C, where temperature was held (30 min). The *n*-alkanes were not isolated from other branched cyclic compounds (hopanes and steranes) since *n*-alkanes formed a major portion of the saturated hydrocarbon fraction and sample material was limited. After *n*-alkane characterization, compound-specific isotope analysis of samples was conducted using a Thermo Trace GC Ultra fitted with a DB-1MS capillary column (same parameters described above) coupled via a GC Isolink and Conflo IV to a Thermo Delta V Advantage isotope ratio MS. The carrier gas for both GC-MS and GC-IRMS was helium (constant flow 1.1 mL/min). $\delta^{13}C$ data are only given when GC baseline separation was achieved for compounds of interest. Each sample was run in triplicate, averaged, and given a standard deviation. The standard used was the Vienna Pee Dee Belemnite (VPDB).

3.2. Bulk organic carbon isotopes and total organic carbon

Powdered rock samples (<0.5 g) were digested in 2M HCl (12 hr) and washed with Milli-Q water (until neutral) to remove carbonates. Samples were freeze-dried (12 hr) to remove residual water. Elemental (total organic carbon) and isotopic ($\delta^{13}C_{org}$) analyses were undertaken at the West Australian Biogeochemistry Centre, University of Western Australia under Grzegorz Skrzypek using a CHNS elemental analyzer and Delta V Plus MS connected to a Thermo Flash 1112 via a Conflo IV. Full details in Skrzypek (2013). The standard used was the VPDB.

4. PAHs in the ETE

Before detailing the results of this study, it is pertinent to understand how pyPAH distributions and their ratios are used to support wildfire activity during the ETE. Fig. 2 provides a summary of PAHs and charcoal evidence during the ETE with expanded profiles of sections closest to the SW UK. Increases in pyPAHs across Greenland, Poland, and China were attributed to evidence of paleowildfire (Fang et al., 2021; Marynowski and Simoneit, 2009; Song et al., 2020; Williford et al., 2014; Zhang et al., 2020), similar to other mass extinction events e.g., the end-Permian (Nabbefeld et al., 2010; Shen et al., 2011). However, pyPAHs at Mariental-1, NW Germany were instead attributed directly to CAMP activity, possibly CAMP intrusions into coal beds, rather than CAMP-induced biomass burning (van de Schootbrugge et al., 2009) due to elevated concentrations of coronene and increases in the ratio of coronene to benzo(*a*)pyrene (Cor/BaP; values of 3.46). This hypothesis was based on 1) an absence of charcoal; 2) darkened palynomorphs in the Trilete beds attributed to CAMP-induced soil acidification and/or sulphuric acid depositions (van de Schootbrugge et al., 2009); and 3) burn experiment data in which biomass burning resulted in both low concentrations of coronene and low ratios of Cor/BaP (Freeman and Cattell, 1990). Similar Cor/BaP increases were also observed at Astartekløft, East Greenland (2.15) (Williford et al., 2014) and even higher ratios were observed at Kamień Pomorski IG-1, NW Poland (24.5) where darkened palynomorphs were also reported (Marynowski and Simoneit, 2009; Pieńkowski et al., 2011) (Fig. 2). However, based on other and more recent findings, pyPAH increases at Mariental-1 could instead be attributed to biomass burning rather than a direct signal of the CAMP. For example, periods of intense biomass burning can preferentially form HMW pyrogenic PAHs, including coronene (seven rings), explaining increased Cor/BaP abundances (Finkelstein et al., 2005). Additionally, increases in the pyPAHs benzo(*a*)anthracene and benzo(*ghi*)perylene at Mariental-1 are similar to or greater than those of coronene, a profile consistent with combustion of terrestrial material (Freeman and Cattell, 1990; Karp et al., 2020). Finally, sedimentary charcoal preservation is biased towards high temperature burning events and combustion of woody material but Mariental-1 PAH increases coincide with fern proliferation. Arguably, increases in coronene relative to other combustion-derived PAHs likely reflect more intense burning (Finkelstein et al., 2005). For expanded details on all charcoal and pyPAH bearing ETE sections, see the supplementary information.

5. Results and discussion

5.1. Combustion PAHs and the "initial" CIE

In the SW UK, initial CIE Cor/BaP ratios of 33.70 at St. Audrie's Bay and even greater ratios of 88.20 and 20.93 at Lilstock superficially suggest widespread and intense wildfire activity across Greenland and Europe during deposition of the initial CIE (Fig. 2). However, based on concentrations of pyPAHs and their ratios (described below) other processes are likely responsible, and a more thorough interpretation is required.

Intense biomass burning can lead to the preferential formation of HMW pyPAH (Finkelstein et al., 2005). Thus, comparisons between the relative abundance of HMW and LMW pyPAHs provide details on the activity and intensity of CAMP-induced wildfires. In the initial CIE there are no significant changes in the relative abundance of pyPAHs with differing ring numbers that may be expected with an intense burning event. Additionally, the relative abundance of HMW and LMW pyPAHs is different between the sections. Throughout the St. Audrie's Bay section, the relative abundances of pyPAHs containing three rings (phenanthrene and fluoranthene) and six and seven rings (benzo(*ghi*)perylene and coronene) are higher than those comprised of four rings (benzo(*a*)anthracene, chrysene, and triphenylene) and five rings (benzo(*e*)pyrene and benzo(*a*)pyrene). At Lilstock a different pattern is observed; pyPAHs containing six and seven rings have greatest abundances from the upper Westbury Formation until the termination of the initial CIE, after which pyPAHs comprised of three rings have highest abundance (Fig. 3). These data show different PAH regimes between sections, however, discrepancies between sections due to preferentially degradation of LMW pyPAHs cannot be ruled out (Denis et al., 2021 and refs therein). Additionally, in comparing concentrations of pyPAHs between European sections, concentrations of coronene and benzo(*a*)pyrene are considerably lower at St. Audrie's Bay (coronene av. 0.35 μg/g TOC; benzo(*a*)pyrene av. 0.05 μg/g TOC) and Lilstock (coronene av. 2.04 μg/g TOC; benzo(*a*)pyrene av. 0.01 μg/g TOC) compared to those reported in East Greenland (coronene 7.93 μg/g TOC; benzo(*a*)pyrene 3.70 μg/g TOC) (Williford et al., 2014) and German (coronene 8.38 μg/g TOC; benzo(*a*)pyrene 2.42 μg/g TOC) sections (van de Schootbrugge et al., 2009) (Fig. 2). These data suggest paleowildfires were less intense in the Bristol Channel Basin compared to those reported in other European basins.

To infer changes in wildfire activity we use the sum of combustion-derived PAHs (∑pyPAH; Fig. 3). ∑pyPAH values in-

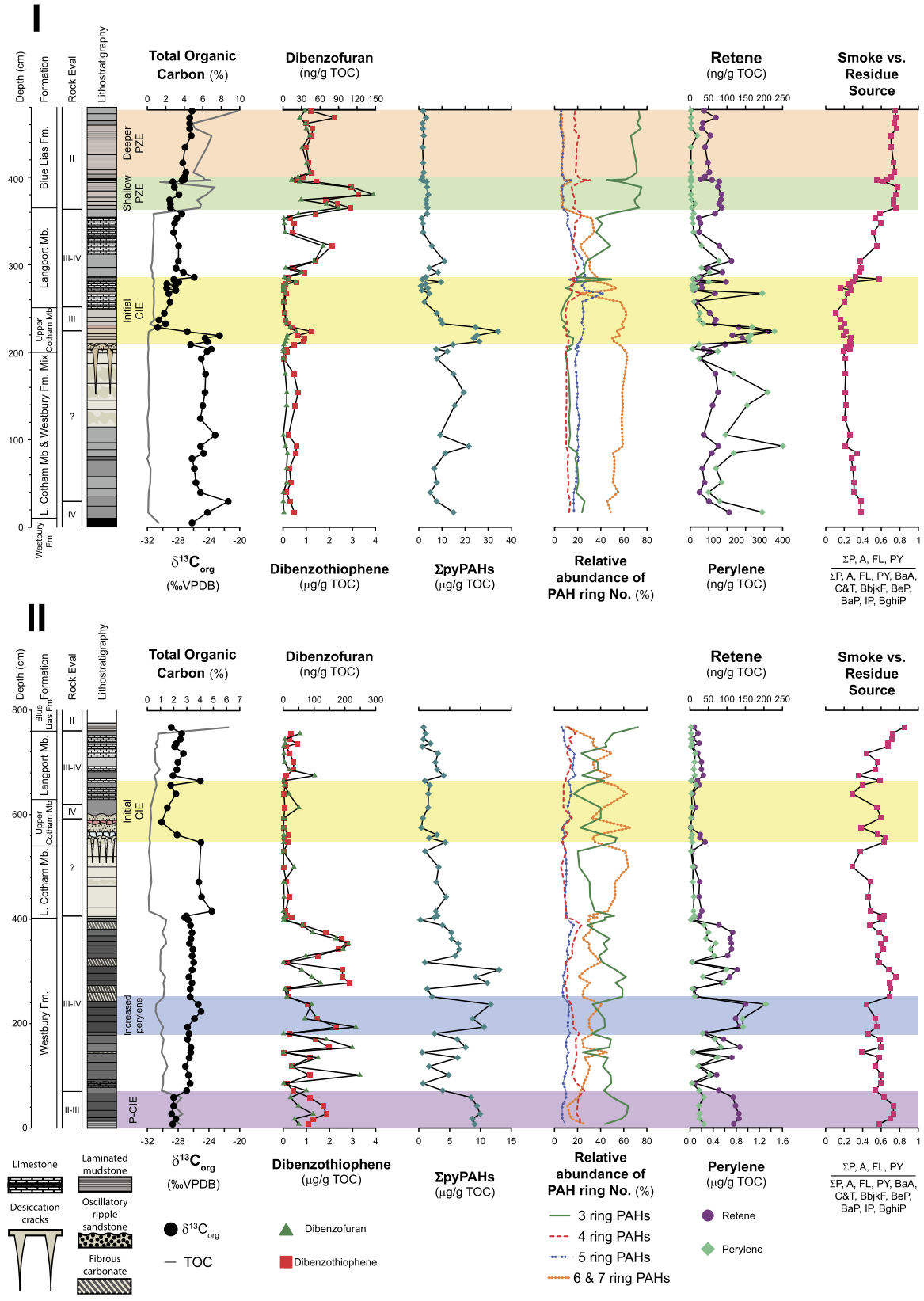

Fig. 3. LMW PAHs, sum of combustion-derived PAHs (∑pyPAH), relative abundance of pyPAHs with differing ring numbers, perylene and retene concentrations, and ratios of PAHs indicative of smoke vs. residue sources at Lilstock (I; upper panel) and St. Audrie's Bay (II; lower panel) relative to the $\delta^{13}C_{org}$ and total organic carbon (TOC) records. Note that perylene is represented as µg/g TOC at St. Audrie's Bay and ng/g TOC at Lilstock. Highlighted areas of interest include the precursor CIE (P-CIE; purple), interval of increased perylene (blue), initial CIE (yellow), photic zone euxinia (PZE) extending further into shallower regions of the photic zone (green), and PZE limited to deeper depths (orange). Combustion Ring No.: 3 rings – phenanthrene and fluoranthene; 4 rings – benzo(*a*)anthracene, chrysene, and triphenylene; 5 rings – benzo(*e*)pyrene and benzo(*a*)pyrene; and six & seven rings – benzo(*ghi*)perylene and coronene. ∑pyPAH is the sum of 3, 4, 5, 6 and 7 ringed PAHs. For PAH abbreviations in smoke vs. residue source see Table 1. Lithology is fully described in section 2 and the supplementary information, with colours representing colour of the strata as observed in the field. Mb – Member; Fm – Formation; P-CIE – precursor CIE; VPDB – Vienna Pee Dee Belemnite. Full Rock-Eval, $\delta^{13}C_{org}$, and TOC record first published in (Fox et al., 2022).

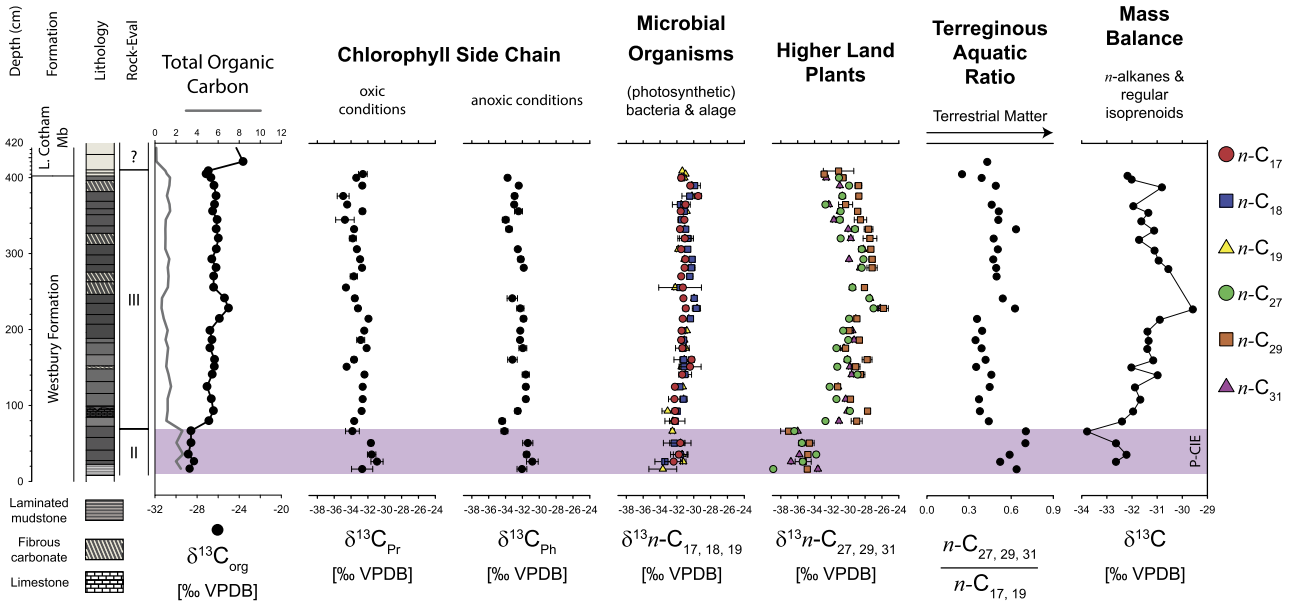

Fig. 4. Compound specific isotopes of regular isoprenoids, short chain *n*-alkanes, and long chain *n*-alkanes with *n*-alkane ratios representing input of terrestrial material and mass balance of regular isoprenoids and *n*-alkanes. Full equation and details on the mass balance equation given in the supplementary information. The precursor CIE (P-CIE) is highlighted in purple. Pr – pristane; Ph – phytane; VPDB - Vienna Pee Dee Belemnite.

crease during the onset of the initial CIE at both St. Audrie's Bay and Lilstock, however, the magnitude is strikingly different between sections. Whereas the ∑pyPAH profile at Lilstock show a distinct, large magnitude, and transient increase (maximum 34.07 μg/g TOC) consistent with a CAMP-induced biomass burning event, the ∑pyPAH profile at St. Audrie's Bay instead displays a lower magnitude and much shorter-lived increase with markedly lower concentrations (max 4.21 μg/g TOC) comparable with concentrations in the lower Cotham Member. Given the close proximity between St. Audrie's Bay and Lilstock (~7 km) and that fire products can travel great distances, smoke aerosols up to ~10,000 km and charred particles up to ~10 km (with impacts of secondary transport important) (Karp et al., 2020), the respective PAH profiles through the initial CIE do not reflect CAMP-induced biomass burning. Increased initial CIE pyPAHs at Lilstock could possibly be related to an extremely localized and small burning event in which pyPAHs did not travel far or, more likely, additional processes were at play (i.e., soil-derived pyPAHs input described in section 5.2).

Together, these data show that through the initial CIE in the SW UK, pyPAHs reflect neither intense nor widespread CAMP-induced biomass burning. During other intervals of LIP-driven biotic crises, such as Ocean Anoxic Event 2, widespread combustion of terrestrial material is thought to have driven negative CIEs similar to the initial CIE (Boudinot and Sepúlveda, 2020). Thus, the discrepancies between SW UK biomass burning records presented in this study further separate the SW UK initial CIE from the CAMP activity (i.e., volcanism-induced biomass burning), as evidenced by other biomarker studies (Beith et al., 2021; Fox et al., 2020). Because HMW pyPAHs are more locally deposited from the source compared to LMW pyPAHs (Karp et al., 2020 and refs therein), increases in HMW pyPAHs in European and East Greenland ETE sections during the initial CIE could represent more intense but localized burning events, rather than widespread burning.

5.2. A terrestrial input origin for the "precursor" CIE

Like the initial CIE, the precursor CIE is routinely used in chemostratigraphic correlations. To better establish the precursor CIE origin(s) in the SW UK, we investigated δ^{13}C values of *n*-alkanes (δ^{13}*n*-C) and the regular isoprenoids pristane and phytane ($\delta^{13}C_{Pr}$ and $\delta^{13}C_{Ph}$, respectively) alongside PAH abundances through the Westbury Formation (Fig. 3; 4). Hopane and sterane biomarker abundances during this interval are reported in in the supplemental information of Fox et al. (2022). Of all measured compound-specific isotopes the n-$C_{27,29,31}$, sourced from land plant waxes (Eglinton et al., 1962), most closely follow the trends observed in the $\delta^{13}C_{org}$ record; $\delta^{13}n$-$C_{27,29,31}$ values are the most negative (ranging between ~ -34‰ and -39‰) during the precursor CIE and at its termination exhibit an ~8‰ positive shift synchronous to positive shifts in the $\delta^{13}C_{org}$ record (Fig. 4). Values of $\delta^{13}C_{Pr}$ and $\delta^{13}C_{Ph}$, largely derived from chlorophyll *a* and *b* (Powell and McKirdy, 1973), are more ^{13}C-enriched compared to $\delta^{13}n$-$C_{27,29,31}$ values throughout the precursor CIE and shift negatively at the precursor CIE termination whereas values of $\delta^{13}n$-C_{17-19}, indicative of algae and (photosynthetic) bacteria (Cranwell et al., 1987; Grice et al., 2005), show negligible change (Fig. 4). The absence of synchronous negative δ^{13}C shifts at the precursor CIE in all biomarkers suggests the precursor CIE is not of an exogenous (i.e., CAMP) origin. Instead, based on isotopic compositions and PAH abundances the precursor CIE is best attributed to the input of land plants depleted in ^{13}C.

The relative abundance of long chain *n*-alkanes from land plant leaf waxes and concentrations of the PAH retene that can derive from conifer resins (Villar et al., 1988) serve as proxies for input of land plant material to the sedimentary record. We find increases in long-chain *n*-alkanes compared to short-chain *n*-alkanes (terrigenous vs. aquatic ratio; Fig. 4) and elevated retene concentrations in the precursor CIE (Fig. 3) coeval with the most negative $\delta^{13}n$-$C_{27,29,31}$ values (Fig. 2). Additionally, a mass balance equation (supplementary information) using the relative abundance and isotopic compositions of pristane, phytane and n-$C_{17,18,19,27,29,31}$ generally shows more depleted δ^{13}C values in the precursor CIE (Fig. 4). These data support greater input of isotopically light land plant material to the sedimentary record driving the precursor CIE.

The increased retene concentrations in the precursor CIE and the cyclical fluctuations throughout the remaining Westbury Formation are also observed in the ∑pyPAH profiles and the LMW PAHs dibenzothiophene (DBT) and dibenzofuran (DBF) (Fig. 3). The good correlation ($r^2 = 0.77$) between ∑pyPAH and total concen-

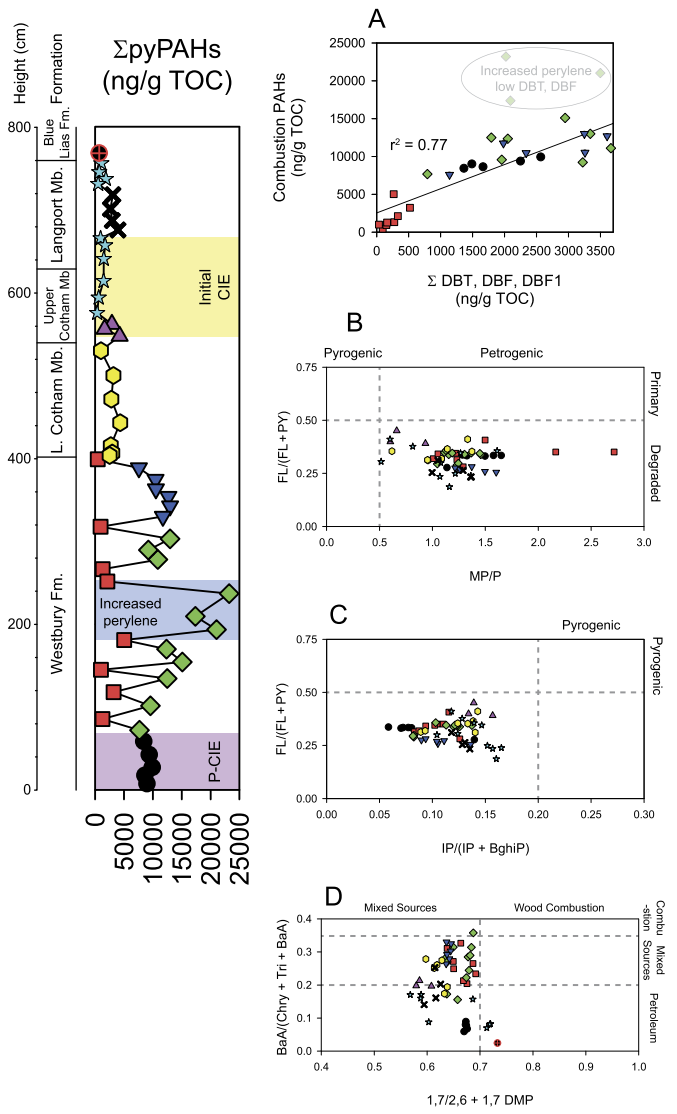

Fig. 5. PAHs ratios at St. Audrie's Bay. Left shows the sum of combustion PAHs (∑pyPAH) relative to formation changes. A: Correlation between the sum of combustion PAHs and sum of DBF, DBT and methyl-DBF compounds. Those samples within the increased perylene interval are excluded in this correlation and are represented by greyscale diamonds. B: Pyrogenic vs. petrogenic and primary vs. degraded PAHs based on Karp et al. (2018). C: Pyrogenic vs. petrogenic source based on Song et al. (2020). D: Mixed sources and combustion based on Yunker et al. (2002). Symbols in the ∑pyPAH profile match those used in ratio plots. Abbreviations described in Table 1.

trations of DBT, DBF and their methylated homologues throughout the Westbury Formation supports a common source or process (Fig. 5A). Here we consider the meaning of such fluctuations.

DBT and DBF are argued to track enhanced input of terrestrial material by soil erosion (Fenton et al., 2007; Kaiho et al., 2016; Sephton et al., 2005). Additionally, DBF shows evidence for a terrestrial origin forming by dehydration (biodegradation) of cellulose indicating the presence of polysaccharides in organic matter (Sephton et al., 2005 and refs therein) and DBT and DBF are proposed to have a common lignin source (Fenton et al., 2007 and refs therein). These data suggest cyclical inputs of terrestrial material to the marine realm are responsible for the DBT and DBF fluctuations in the Westbury Formation. Modern studies and those on ocean anoxic events have found that biomass burning events are associated with increased terrestrial material to the marine realm via riverine and aerosol transport (Boudinot and Sepúlveda, 2020 and references therein). Therefore, cyclical increases in PAHs in the Westbury Formation at St. Audrie's Bay could represent fire events driving input of terrestrial material. However, origins of pyPAHs must be considered.

PAH ratios used in modern analogues to determine petrogenic (i.e., oil/coal-related) vs. pyrogenic (fire) origins for pyPAHs were successfully applied in ancient PAH studies to show pyrogenic origins for pyPAHs (e.g., Karp et al., 2018; Song et al., 2020). These ratios include phenanthrene to methylated phenanthrene isomers, fluoranthene/pyrene + fluoranthene, and Indeno[1,2,3-cd]pyrene/benzo(*ghi*)perylene + Indeno[1,2,3-cd]pyrene (see Stogiannidis and Laane, 2015). pyPAHs in the Westbury Formation at St. Audrie's Bay mostly fall in the petrogenic range (Figs. 5; Supplemental information) suggesting these pyPAHs increases are not related to combustion at the time of deposition. Since PAHs readily adsorb onto atmospheric and soil particles, Westbury Formation pyPAH increases could be associated with terrestrial input of older soil-stored pyPAHs rather than fire at the time of deposition, supported by co-occurring increases in DBT and DBF. Furthermore, when considering the smoke vs. residue signal, i.e., the ratio of LMW pyPAHs to LMW and HMW pyPAHs, (Karp et al., 2020) values in the Westbury Formation are below 0.8 (Fig. 3), suggesting a residue source and an abundance of pyPAHs that do not travel far. However, a mixed pyrogenic and petrogenic origin for Westbury Formation pyPAHs cannot be entirely ruled out; ratios of 1,7/2,6 + dimethylphenanthrene plot mostly as mixed source and close to a wood combustion source and ratios of benzo(*a*)anthracene/chrysene + triphenylene + benzo(*a*)anthracene also show mixed source origins (Fig. 5). Additionally, relative abundance of PAHs and their methylated isomers (Fig. 6) are similar to those of mixed petrographic and pyrogenic sources from modern analogues (Stogiannidis and Laane, 2015), i.e., similar concentrations between phenanthrene, pyrene, and fluoranthene and their methylated homologues alongside abundant of five- and six-ringed pyPAHs. The ratio of fluoranthene/pyrene + fluoranthene doubles as a proxy for primary vs. degraded PAHs (Karp et al., 2018), for which all St. Audrie's Bay samples show a degraded/petrogenic source. As soil and marine bacteria preferentially degrade fluoranthene over pyrene (Arias et al., 2017; Karp et al., 2018 and references therein), it is difficult to discern whether pyPAHs are sourced from fire at the time of deposition and subsequently degraded in the marine realm, or the remnants of older fire events that were degraded in soils, or a combination of both. Additionally, the smoke vs. residue proxy may also be skewed towards lower values due to degradation of LMW pyPAHs such as phenanthrene and fluoranthene (e.g., Denis et al., 2021).

Since only two of the six PAH ratios used to determine petrogenic vs. pyrogenic sources in the Westbury Formation support mixed sources and none show a combustion origin (Fig. 5; Supplementary information) we consider pyPAH profiles evidence of erosional release of older soil-stored PAHs and terrestrial material at this interval. pyPAHs increases during the Westbury Formation related to enhanced input of terrestrial material are supported by other geochemical observations such as elevated $^{182}Os/^{188}Os_{(i)}$ isotope values in the Westbury Formation (Cohen and Coe, 2002). Regardless of the exact mechanism, the PAH-evidenced increases in terrestrial material in addition to compound-specific isotope data further supports increased input of ^{13}C-depleted terrestrial plant material driving the precursor CIE.

For much of the Westbury Formation, perylene concentrations also track the cyclical changes in DBT, DBF and ∑pyPAH, with the exception of one interval where the largest perylene increases (parallel with increases in pyPAHs) coincide with low DBT and DBF concentrations. Isotopic analyses and changes in perylene concentrations with lignin alcohol ratios show strongest evidence that the formation of perylene is associated with lignin degradation and originate from wood-degrading fungi (Grice et al., 2009). Increases

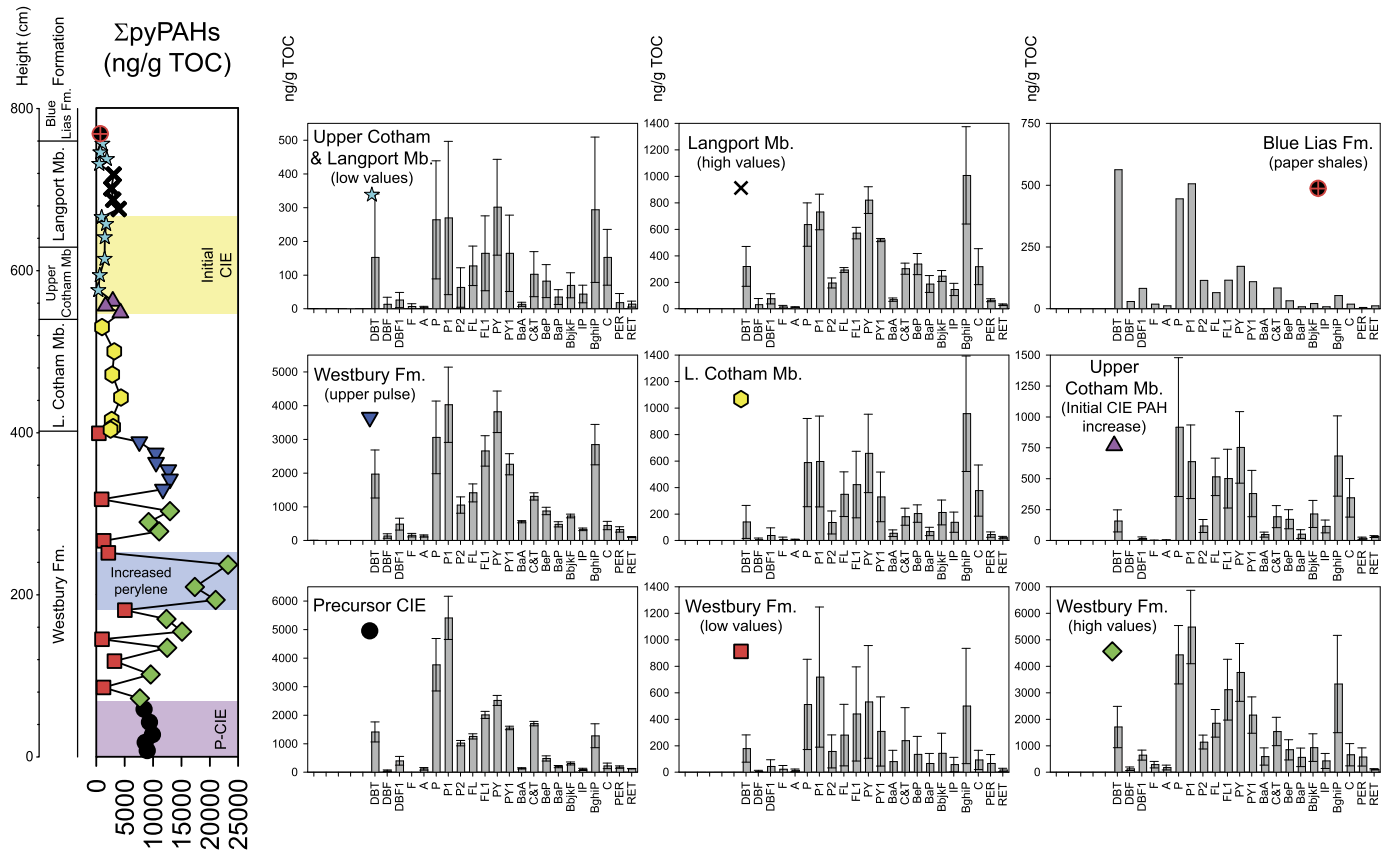

Fig. 6. PAHs at St. Audrie's Bay. Left shows the sum of combustion-derived PAHs (∑pyPAH) relative to formation changes. Bar plots to the right represent the average value of individual compounds in ng/g TOC with standard deviation across select intervals. Symbols in bar plots match those in the ∑pyPAH profile and indicate which samples were averaged. Note that methylated phenanthrene compounds (P1) are given by 1- and 2- methylphenanthrene. Compound abbreviations are given in Table 1. Highlighted intervals correspond to those of Fig. 3. Abbreviations: Mb – Member; Fm – Formation; L – lower.

in perylene coincident with reductions in DBT and DBF further supports evidence that perylene is associated with the degradation of lignin and that DBT and DBF have a common lignin source as well as a terrestrial control on the cyclical increases in ∑pyPAH concentrations in the Westbury Formation and thus terrestrial input during the precursor CIE. Terrestrial controls on pyPAHs may also account for the discrepancies in the ∑pyPAH concentrations between Lilstock and St. Audrie's Bay during the initial CIE. Large and abrupt increases in ∑pyPAH concentrations at Lilstock coincide with only minor increases in DBT and DBF concentrations but large increases in perylene concentrations supporting increased terrestrial material and lignin degradation (thus reduced DBT and DBF concentrations) whereas little to no changes are observed in concentrations of ∑pyPAH, perylene, DBT, or DBF at St. Audrie's Bay. Additionally, petrogenic vs. pyrogenic PAH ratios during the CIE at Lilstock are similar to those of the Westbury Formation at St. Audrie's Bay (Figs. 5–8).

The precursor CIE is marked by higher total organic carbon (TOC) percentages (~1.5% difference) and changes in organic matter type (e.g., a shift from Rock-Eval type II-III to III-IV) (Fig. 3; 4). These results, combined with the result of a modification in land plant input, demonstrate the precursor CIE does not reflect release of isotopically light carbon. Instead, these changes suggest C_3 plant community change involving a greater input of ^{13}C-depleted terrestrial plant material. Linking CAMP eruptions to the SW UK relies on chemostratigraphic correlations (e.g. Lindström et al., 2017) with non-unique solutions. Effects of CAMP-outgassed CO_2 and global warming, such as water column stratification, and other ecological stresses are not observed during the precursor CIE (Fox et al., 2022). Furthermore, paleomagnetic correlations of the Westbury Formation (Hounslow et al., 2004; Kent et al., 2017) suggest the precursor CIE falls within magnetochron E22n and would have an age of 203-203.5 Ma, more than a million years older than the oldest known CAMP eruptions (201.635±0.029 Ma) (Davies et al., 2017. Thus, introduction of ^{13}C-depleted CO_2 by CAMP processes can be excluded as a cause for the precursor CIE. This finding, in addition to the recent data supporting that the initial and main CIEs in the SW UK are also unrelated to CAMP activity (Fox et al., 2020), point to the significant impacts of local factors on the $\delta^{13}C_{org}$ record. Correlations by chemostratigraphic means alone are problematic for the ETE, particularly those that correlate to the SW UK, and possibly other mass extinction and biotic turnover events where $\delta^{13}C_{org}$ anomalies are directly associated with large igneous provinces.

5.3. PAHs and soil erosion evidence in the extinction horizon

The ETE horizon we favour in the Bristol Channel Basin is in the lowermost Blue Lias Formation (paper shales; see section 2). Here, two paleodepositional environments related to changes in redox are evident; one at the extinction horizon where photic zone euxinia (PZE) was most vertically intensified, and another directly following, where PZE is restricted to lower regions of the water column (Fox et al., 2022). Two notable changes in PAH profiles are apparent at this interval. The first is a large short-lived increase in the LMW PAHs DBT and DBF within the paleodepositional environment exhibiting shoaled PZE, the second is a shift in the relative abundance of pyPAHs to those containing three rings (phenanthrene and fluoranthene) throughout both redox intervals. We ascribe these increases to soil erosion and smoke signals, respectively (described below).

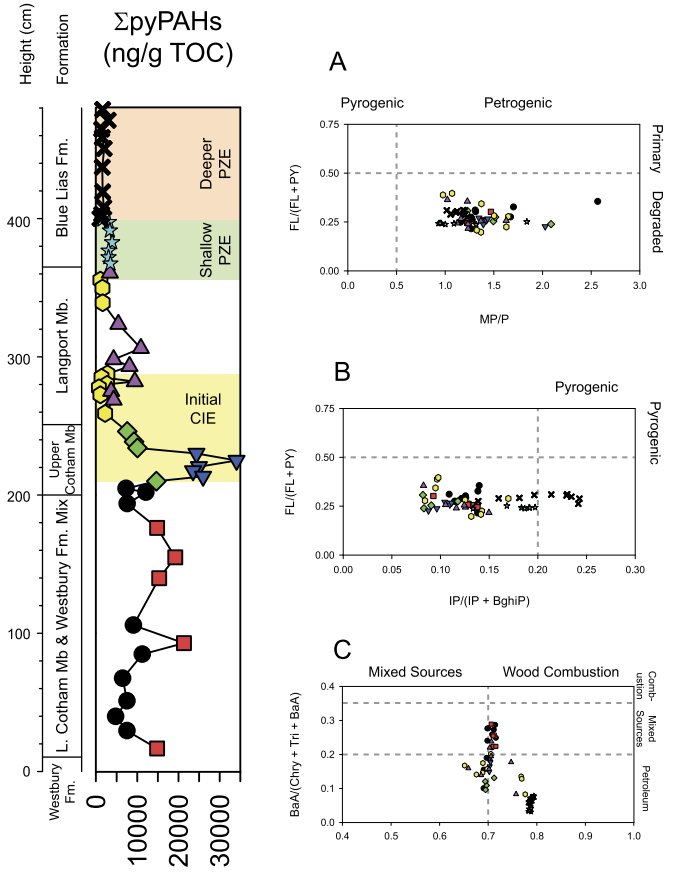

Fig. 7. PAH ratios at Lilstock. Left shows the sum of combustion-derived PAHs (∑pyPAH) relative to formation changes. A: Pyrogenic vs. petrogenic and primary vs. degraded PAHs based on Karp et al. (2018). B: Pyrogenic vs. petrogenic source based on Song et al. (2020). C: Mixed sources and combustion based on Yunker et al. (2002). Symbols in the ∑pyPAH profile match those used in ratio plots. Abbreviations described in Table 1.

During the end-Permian extinction, dysoxic and sulfidic bottom water redox conditions that formed prior to marine ecosystem collapse allowed for DBT and DBF formation, and subsequent shifts to anoxic (possibly euxinic) conditions hindered the formation of these compounds (Fenton et al., 2007). Since increases in DBT and DBF occur during most intense PZE conditions and the marine expression of the ETE, DBT and DBF concentrations cannot be related to increases prior to marine ecosystem collapse (Fenton et al., 2007; Sephton et al., 2005). We instead suggest a soil erosion event is responsible for increases in DBT and DBF. Enhanced input of terrestrial material by soil erosion during other mass extinction events accounts for increases in LMW PAHs including DBT and DBF that helps drive marine anoxia (e.g., Kaiho et al., 2016). Such PAH increases and redox conditions are readily observed in the SW UK during the marine extinction (Fig. 3) and are further supported by increases in *n*-alkanes indicative of terrestrial material (supplementary information). Additionally, trends in biomarkers and their inferred redox conditions in the paper shales are similar to those found during the soil erosion event(s) at the end-Permian mass extinction in China and Northern Italy (Kaiho et al., 2016; Sephton et al., 2005). These include increases in DBF and its methylated isomers, increases in DBF relative to biomass burning compounds, low pristane to phytane ratios and C_{35} homohopane index between 5 and 10% (redox parameters), high gammacerane index (stratification proxy), and increases in DBT. Soil erosion, identified through reworking of pollen assemblages across ETE European sections, has recently proved important as an extinction mechanism for terrestrial species and connecting ecosystem perturbations across terrestrial and aquatic realms (van de Schootbrugge et al., 2020).

Soil erosion can be enhanced by a variety of different processes, including tectonic events (earthquakes), biomass burning, increased precipitation, and soil acidification (van de Schootbrugge et al., 2020). Evidence of earthquakes in the SW UK, in the form of seismites, occur much lower in the stratigraphic column alongside desiccation cracks and at the onset of the initial CIE (Fig. 2). ∑pyPAH concentrations show little change in the Blue Lias Formation and only minor increases in the lowermost Blue Lias Formation (where DBT and DBF concentrations are highest) suggest biomass burning is not responsible for driving soil erosion and increased input of terrestrial material. Furthermore, highest values of the smoke vs. residue proxy in the paper shales (Fig. 3) suggests that fire activity was not in close proximity to the depositional environment.

Soil erosion *via* acid rain is circumstantial during the ETE. Evidence consists of darkened spores and pollen from various European sections (Pieńkowski et al., 2011; van de Schootbrugge et al., 2009). Pollen and spore colouration and reworked palynomorph percentages are yet to be investigated in the SW UK (Bonis et al., 2010). Based on chemostratigraphy and biostratigraphy, CIE correlations between the SW UK and Germany typically correlate the Bristol Channel Basin initial CIE and the CIE above the Trilete beds in Mariental-1. Arguably, based on palynology, the CIE in Mariental-1 could be correlated to the minor excursion in paper shales deposited during the extinction event; see Fig. 13 in Lindström et al. (2017). This would place the soil acidification event and elevated PAH abundances in NW Europe and terrestrial and marine ecosystem perturbations in the SW UK in closer proximity to one another, better linking CAMP environmental perturbations and indicating a plausible fire source for the smoke signal recorded in the paper shales. Such a soil acidification event coincident with the tripartite of stressors driving the marine extinction links CAMP-driven terrestrial and marine ecosystem stresses accounting for the ETE. However, changes in $\delta^{13}C_{org}$ profiles can have sources other than those from the CAMP (Fox et al., 2020) so such correlations should be used in caution and changes in palynology across European sections vary in both order of first and last occurrences and relative to the $\delta^{13}C_{org}$ record.

In the Blue Lias Formation, the shift to a smoke source in the smoke vs. fire proxy and minor increases in ∑pyPAH are largely driven by changes in phenanthrene (Fig. 3; 6; 8; Supplementary Information). These increases coincide with the best evidence of biomass burning in PAH ratios across both sections and all investigated intervals in the SW UK (Fig. 5; 7). Since the increase in LMW pyPAHs is interpreted to represent a smoke signal with the potential to travel distances of up to 10,000 km (Karp et al., 2020), these increases best represent CAMP-driven wildfire coincident with other major terrestrial (soil erosion) and marine (intensified PZE and acidification) ecological perturbations. Major contributions of phenanthrene in other ETE PAH profiles may also reflect smoke signals (Fang et al., 2021; Marynowski and Simoneit, 2009; Song et al., 2020; Zhang et al., 2020). Although PAH ratios suggest a pyrogenic origin, increases may also be related to redox conditions and preservation potential; phenanthrene is a readily biodegradable PAH, more so compared to HMW PAHs (Arias et al., 2017 and references therein; Denis et al., 2021), thus the combination of ecological stressors in the lower Blue Lias Formation may inhibit phenanthrene degradation and account for large increases.

Importantly, all PAH compounds are normalized to TOC throughout the record. High TOC percentages in the lower Blue Lias Formation are due to marine conditions favouring carbon burial and increases in marine organic matter input, thus, changes in terrestrial signals in this interval are likely masked more so than those stratigraphic intervals below, somewhat hindering compar-

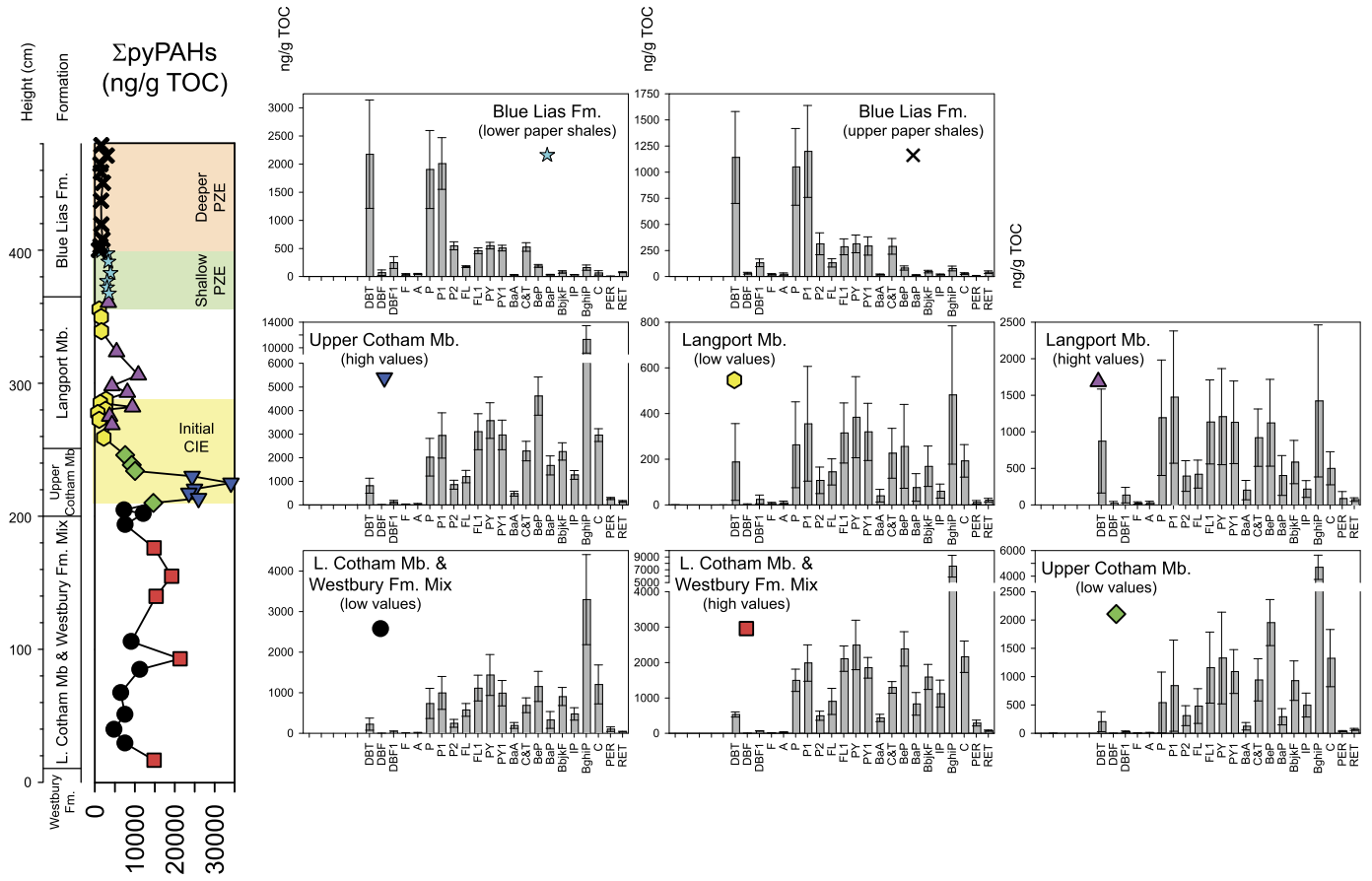

Fig. 8. PAHs at Lilstock. Left shows the sum of combustion-derived PAHs (∑pyPAH) relative to formation changes. Bar plots to the right represent the average value of individual compounds in ng/g TOC with standard deviation across select intervals. Symbols in bar plots match those in the ∑pyPAH profile and indicate which samples were averaged. Note that methylated phenanthrene compounds (P1) are given by 1- and 2- methylphenanthrene. Compound abbreviations are given in Table 1. Highlighted intervals correspond to those of Fig. 3. Abbreviations: Mb – Member; Fm – Formation; L – lower.

isons between formations in the same section due to rapid changes in environment. Regardless, the largest increases in DBT and DBF occur in the lower Blue Lias Formation, indicating soil erosion processes pose a larger terrestrial ecosystem stress than biomass burning in the SW UK.

6. Conclusions

Notwithstanding evidence from European and Greenland ETE sections for wildfire activity through shifts in palynology and extinction, the PAH profiles in the ETE sections from SW UK reveal that biomass burning is not a major source of PAHs. Instead, the extinction horizon in these sections (lower Blue Lias Formation) is associated with a soil erosion event and distant smoke signals of wildfires that links the CAMP-driven terrestrial and marine ecosystem perturbations, providing the best evidence of catastrophic effects of the CAMP volcanism throughout the latest Rhaetian. Increases in the abundance of LMW pyPAHs at this interval point to a distal burn signal, suggesting that if fire events were the source of LMW pyPAHs, they were not in close proximity to the SW UK.

For the so-called precursor CIE that is routinely used in global chemostratigraphic correlations among ETE sections, the PAH distributions combined with compound-specific isotope data show this interval is not a result of the CAMP activity. For the initial CIE interval, discrepancies in the concentration of total combustion-derived PAHs among geographically close (∼7 km) localities suggest the signal there is not associated with regional biomass burning. The observed differences could be attributed to erosion and soil-stored PAHs, the process likely responsible for the cyclical increases in LMW PAHs and indicative of contributions from terrestrial material below the initial CIE in the Westbury Formation. Of these cyclical increases, one interval is characterized by terrestrial material depleted in ^{13}C relative to marine phytoplankton. These terrestrial contributions, combined with changes in organic matter type and organic carbon percentages, are likely responsible for the precursor CIE.

The results of this study show that a characterization of a fuller range of PAHs and their ratios can provide important insights into the many factors that have contributed to the ETE, and potentially to other periods of biotic crises driven by LIPs. Further detailed high-resolution studies utilizing a similar comprehensive sampling of the available PAHs (more than just those mostly associated with biomass burning) will lead to important contributions to both the characterization of paleoenvironments during the ETE and gauging the far-field effects of CAMP volcanism.

CRediT authorship contribution statement

C. P. Fox: Conceptualization, Formal Analysis, Investigation, Writing - Original Draft, Writing - Review and Editing, Visualization. **J.H. Whiteside:** Conceptualization, Investigation, Writing - Original Draft, Visualization, Supervision. **P. E. Olsen:** Conceptualization, Investigation, Writing - Review and Editing, Visualization. **K. Grice:** Conceptualization, Formal Analysis, Investigation, Resources, Writing - Original Draft, Writing - Review and Editing, Visualization, Main Supervision.

Declaration of competing interest

The authors declare that they have no known competing financial interests or personal relationships that could have appeared to influence the work reported in this paper.

Acknowledgements

We acknowledge Peter Hopper, Alex Holman, and P. Sargent Bray for technical support and Leszek Marynowski for providing additional PAH data from their 2009 publication. **Funding:** Fox acknowledges Curtin University, the European Association of Organic Geochemistry, and Khalifa University of Science and Technology (CIRA-2019-066). Fox and Grice thank the ARC (LP150100341; LE110100119; LE100100041; LE0882836). Whiteside thanks the NSF (EAR 1147402). Olsen acknowledges the Lamont Climate Center.

Appendix A. Supplementary material

Supplementary material related to this article can be found online at https://doi.org/10.1016/j.epsl.2022.117418.

References

Alipour, M., Alizadeh, B., Jahangard, A., GandomiSani, A., 2021. Wildfire events at the Triassic–Jurassic boundary of the Tabas Basin, Central Iran. Int. J. Coal Sci. Technol. 8, 897–907. https://doi.org/10.1007/s40789-021-00436-2.

Arias, A.H., Souissi, A., Glippa, O., Roussin, M., Dumoulin, D., Net, S., Ouddane, B., Souissi, S., 2017. Removal and biodegradation of phenanthrene, fluoranthene and pyrene by the marine algae rhodomonas baltica enriched from North Atlantic coasts. Bull. Environ. Contam. Toxicol. 98, 392–399. https://doi.org/10.1007/s00128-016-1967-4.

Beith, S.J., Fox, C.P., Marshall, J.E.A., Whiteside, J.H., 2021. Recurring photic zone euxinia in the northwest Tethys impinged end-Triassic recovery. Palaeogeogr. Palaeoclimatol. Palaeoecol. 584, 110680. https://doi.org/10.1016/j.palaeo.2021.110680.

Belcher, C.M., Mander, L., Rein, G., Jervis, F.X., Haworth, M., Hesselbo, S.P., Glasspool, I.J., McElwain, J.C., 2010. Increased fire activity at the Triassic/Jurassic boundary in Greenland due to climate-driven floral change. Nat. Geosci. 3, 426–429. https://doi.org/10.1038/ngeo871.

Bonis, N.R., Ruhl, M., Kürschner, W.M., 2010. Milankovitch-scale palynological turnover across the Triassic–Jurassic transition at St. Audrie's Bay, SW UK. J. Geol. Soc. 167, 877–888. https://doi.org/10.1144/0016-76492009-141.

Boudinot, F.G., Sepúlveda, J., 2020. Marine organic carbon burial increased forest fire frequency during Oceanic Anoxic Event 2. Nat. Geosci. 13, 693–698. https://doi.org/10.1038/s41561-020-0633-y.

Cohen, A.S., Coe, A.L., 2002. New geochemical evidence for the onset of volcanism in the Central Atlantic magmatic province and environmental change at the Triassic-Jurassic boundary. Geology 30, 267–270. https://doi.org/10.1130/0091-7613(2002)030<0267:NGEFTO>2.0.CO;2.

Cranwell, P.A., Eglinton, G., Robinson, N., 1987. Lipids of aquatic organisms as potential contributors to lacustrine sediments—II. Org. Geochem. 11, 513–527. https://doi.org/10.1016/0146-6380(87)90007-6.

Davies, J.H.F.L., Marzoli, A., Bertrand, H., Youbi, N., Ernesto, M., Schaltegger, U., 2017. End-Triassic mass extinction started by intrusive CAMP activity. Nat. Commun. 8, 15596. https://doi.org/10.1038/ncomms15596.

Denis, E.H., Maibauer, B.J., Bowen, G.J., Jardine, P.E., Harrington, G.J., Baczynski, A.A., McInerney, F.A., Collinson, M.E., Belcher, C.M., Wing, S.L., Freeman, K.H., 2021. Decreased soil carbon in a warming world: degraded pyrogenic carbon during the Paleocene-Eocene thermal maximum, Bighorn Basin, Wyoming. Earth Planet. Sci. Lett. 566, 116970. https://doi.org/10.1016/j.epsl.2021.116970.

Dickman, C., McDonald, T., 2020. Some personal reflections on the present and future of Australia's fauna in an increasingly fire-prone continent. Ecol. Manag. Restor. 21, 86–96. https://doi.org/10.1111/emr.12403.

Eglinton, G., Gonzalez, A.G., Hamilton, R.J., Raphael, R.A., 1962. Hydrocarbon constituents of the wax coatings of plant leaves: a taxonomic survey. Phytochemistry 1, 89–102. https://doi.org/10.1016/S0031-9422(00)88006-1.

Fang, Y., Fang, L., Deng, S., Lu, Y., Wang, B., Zhao, X., Wang, Y., Zhang, H., Zhang, X., Sha, J., 2021. Carbon isotope stratigraphy across the Triassic-Jurassic boundary in the high-latitude terrestrial Junggar Basin, NW China. Palaeogeogr. Palaeoclimatol. Palaeoecol. 577, 110559. https://doi.org/10.1016/j.palaeo.2021.110559.

Fenton, S., Grice, K., Twitchett, R.J., Böttcher, M.E., Looy, C.V., Nabbefeld, B., 2007. Changes in biomarker abundances and sulfur isotopes of pyrite across the Permian–Triassic (P/Tr) Schuchert Dal section (East Greenland). Earth Planet. Sci. Lett. 262, 230–239. https://doi.org/10.1016/j.epsl.2007.07.033.

Finkelstein, D.B., Pratt, L.M., Curtin, T.M., Brassell, S.C., 2005. Wildfires and seasonal aridity recorded in Late Cretaceous strata from south-eastern Arizona, USA. Sedimentology 52, 587–599. https://doi.org/10.1111/j.1365-3091.2005.00712.x.

Fox, C.P., Cui, X., Whiteside, J.H., Olsen, P.E., Summons, R.E., Grice, K., 2020. Molecular and isotopic evidence reveals the end-Triassic carbon isotope excursion is not from massive exogenous light carbon. Proc. Natl. Acad. Sci. 117, 30171–30178. https://doi.org/10.1073/pnas.1917661117.

Fox, C.P., Whiteside, J.H., Olsen, P.E., Cui, X., Summons, R.E., Idiz, E., Grice, K., 2022. Two-pronged kill mechanism at the end-Triassic mass extinction. Geology. https://doi.org/10.1130/G49560.1.

Freeman, D.J., Cattell, F.C.R., 1990. Woodburning as a source of atmospheric polycyclic aromatic hydrocarbons. Environ. Sci. Technol. 24, 1581–1585. https://doi.org/10.1021/es00080a019.

Grice, K., Cao, C., Love, G.D., Böttcher, M.E., Twitchett, R.J., Grosjean, E., Summons, R.E., Turgeon, S.C., Dunning, W., Jin, Y., 2005. Photic zone euxinia euring the Permian-Triassic superanoxic event. Science 307 (5710), 706–709. https://doi.org/10.1126/science.1104323.

Grice, K., Lu, H., Atahan, P., Asif, M., Hallmann, C., Greenwood, P., Maslen, E., Tulipani, S., Williford, K., Dodson, J., 2009. New insights into the origin of perylene in geological samples. Geochim. Cosmochim. Acta 73, 6531–6543. https://doi.org/10.1016/j.gca.2009.07.029.

Harris, T.M., 1958. Forest fire in the Mesozoic. J. Ecol. 46, 447–453. https://doi.org/10.2307/2257405.

Hesselbo, S.P., Robinson, S.A., Surlyk, F., 2004. Sea-level change and facies development across potential Triassic–Jurassic boundary horizons, SW Britain. J. Geol. Soc. 161, 365–379. https://doi.org/10.1144/0016-764903-033.

Hesselbo, S.P., Robinson, S.A., Surlyk, F., Piasecki, S., 2002. Terrestrial and marine extinction at the Triassic-Jurassic boundary synchronized with major carbon-cycle perturbation: a link to initiation of massive volcanism? Geology 30, 251–254.

Heunisch, C., Luppold, F.W., Reinhardt, L., Röhling, H.-G., 2010. Palynofazies, Bio- und Lithostratigrafie im Grenzbereich Trias/Jura in der Bohrung Mariental 1 (Lappwaldmulde, Ostniedersachsen). Z. Dt. Ges. Geowiss. 161, 51–98. https://doi.org/10.1127/1860-1804/2010/0161-0051.

Holman, A.I., Grice, K., 2018. δ^{13}C of aromatic compounds in sediments, oils and atmospheric emissions: a review. Org. Geochem. 123, 27–37. https://doi.org/10.1016/j.orggeochem.2018.06.004.

Hounslow, M.W., Posen, P.E., Warrington, G., 2004. Magnetostratigraphy and biostratigraphy of the upper Triassic and lowermost Jurassic succession, St. Audrie's Bay, UK. Palaeogeogr. Palaeoclimatol. Palaeoecol. 213, 331–358. https://doi.org/10.1016/j.palaeo.2004.07.018.

Kaiho, K., Saito, R., Ito, K., Miyaji, T., Biswas, R., Tian, L., Sano, H., Shi, Z., Takahashi, S., Tong, J., Liang, L., Oba, M., Nara, F.W., Tsuchiya, N., Chen, Z.-Q., 2016. Effects of soil erosion and anoxic–euxinic ocean in the Permian–Triassic marine crisis. Heliyon 2, e00137. https://doi.org/10.1016/j.heliyon.2016.e00137.

Karp, A.T., Behrensmeyer, A.K., Freeman, K.H., 2018. Grassland fire ecology has roots in the late Miocene. Proc. Natl. Acad. Sci. 115, 12130–12135. https://doi.org/10.1073/pnas.1809758115.

Karp, A.T., Holman, A.I., Hopper, P., Grice, K., Freeman, K.H., 2020. Fire distinguishers: refined interpretations of polycyclic aromatic hydrocarbons for paleo-applications. Geochim. Cosmochim. Acta 289, 93–113. https://doi.org/10.1016/j.gca.2020.08.024.

Kent, D.V., Olsen, P.E., Muttoni, G., 2017. Astrochronostratigraphic polarity time scale (APTS) for the Late Triassic and Early Jurassic from continental sediments and correlation with standard marine stages. Earth-Sci. Rev. 166, 153–180. https://doi.org/10.1016/j.earscirev.2016.12.014.

Lindström, S., van de Schootbrugge, B., Hansen, K.H., Pedersen, G.K., Alsen, P., Thibault, N., Dybkjær, K., Bjerrum, C.J., Nielsen, L.H., 2017. A new correlation of Triassic–Jurassic boundary successions in NW Europe, Nevada and Peru, and the Central Atlantic Magmatic Province: a time-line for the end-Triassic mass extinction. Palaeogeogr. Palaeoclimatol. Palaeoecol. 478, 80–102. https://doi.org/10.1016/j.palaeo.2016.12.025.

Mander, L., Kürschner, W.M., McElwain, J.C., 2013. Palynostratigraphy and vegetation history of the Triassic–Jurassic transition in East Greenland. J. Geol. Soc. 170, 37–46. https://doi.org/10.1144/jgs2012-018.

Mander, L., Twitchett, R.J., Benton, M.J., 2008. Palaeoecology of the Late Triassic extinction event in the SW UK. J. Geol. Soc. 165, 319–332. https://doi.org/10.1144/0016-76492007-029.

Marynowski, L., Simoneit, B.R.T., 2009. Widespread upper Triassic to lower Jurassic wildfire records from Poland: evidence from charcoal and pyrolytic and pyrolytic polycyclic aromatic hydrocarbons. Palaios 24, 785–798.

McElwain, J.C., Wagner, P.J., Hesselbo, S.P., 2009. Fossil plant relative abundances indicate sudden loss of late Triassic biodiversity in East Greenland. Science 80 (324), 1554–1556. https://doi.org/10.1126/science.1171706.

Nabbefeld, B., Grice, K., Summons, R.E., Hays, L.E., Cao, C., 2010. Significance of polycyclic aromatic hydrocarbons (PAHs) in Permian/Triassic boundary sections. Appl. Geochem. 25 (9), 1374–1382.

Pálfy, J., 2003. Volcanism of the Central Atlantic Magmatic Province as a potential driving force in the end-Triassic mass extinction. In: Cent. Atl. Magmat. Prov. Geophys. Monogr. Ser., vol. 136, pp. 255–267.

Petersen, H.I., Lindström, S., 2012. Synchronous wildfire activity rise and mire deforestation at the Triassic–Jurassic boundary. PLoS ONE 7. e47236.

Pieńkowski, G., Niedźwiedzki, G., Waksmundzka, M., 2011. Sedimentological, palynological and geochemical studies of the terrestrial Triassic–Jurassic boundary in northwestern Poland. Geol. Mag. 149, 308–332. https://doi.org/10.1017/S0016756811000914.

Pole, M., Wang, Y., Dong, C., Xie, X., Tian, N., Li, L., Zhou, N., Lu, N., Xie, A., Zhang, X., 2018. Fires and storms—a Triassic–Jurassic transition section in the Sichuan Basin, China. Palaeobiodivers. Palaeoenviron. 98, 29–47. https://doi.org/10.1007/s12549-017-0315-y.

Powell, T.G., McKirdy, D.M., 1973. Relationship between ratio of pristane to phytane, crude oil composition and geological environment in Australia. Nat. Phys. Sci. 243, 37–39. https://doi.org/10.1038/physci243037a0.

Sephton, M.A., Looy, C.V., Brinkhuis, H., Wignall, P.B., de Leeuw, J.W., Visscher, H., 2005. Catastrophic soil erosion during the end-Permian biotic crisis. Geology 33, 941–944. https://doi.org/10.1130/G21784.1.

Shen, W., Sun, Y., Lin, Y., Liu, D., Chai, P., 2011. Evidence for wildfire in the Meishan section and implications for Permian–Triassic events. Geochim. Cosmochim. Acta 75, 1992–2006. https://doi.org/10.1016/j.gca.2011.01.027.

Skrzypek, G., 2013. Normalization procedures and reference material selection in stable HCNOS isotope analyses: an overview. Anal. Bioanal. Chem. 405, 2815–2823. https://doi.org/10.1007/s00216-012-6517-2.

Song, Y., Algeo, T.J., Wu, W., Luo, G., Li, L., Wang, Y., Xie, S., 2020. Distribution of pyrolytic PAHs across the Triassic-Jurassic boundary in the Sichuan Basin, southwestern China: evidence of wildfire outside the Central Atlantic Magmatic Province. Earth-Sci. Rev. 201, 102970. https://doi.org/10.1016/j.earscirev.2019.102970.

Stogiannidis, E., Laane, R., 2015. Source characterization of polycyclic aromatic hydrocarbons by using their molecular indices: an overview of possibilities. In: Whitacre, D.M. (Ed.), Reviews of Environmental Contamination and Toxicology (Vol. 234). Springer, pp. 49–133.

Uhl, D., Montenari, M., 2011. Charcoal as evidence of palaeo-wildfires in the Late Triassic of SW Germany. Geol. J. 46, 34–41. https://doi.org/10.1002/gj.1229.

van de Schootbrugge, B., Bachan, A., Suan, G., Richoz, S., Payne, J.L., 2013. Microbes, mud and methane: cause and consequence of recurrent Early Jurassic anoxia following the end-Triassic mass extinction. Palaeontology 56, 685–709. https://doi.org/10.1111/pala.12034.

van de Schootbrugge, B., Quan, T.M., Lindström, S., Püttmann, W., Heunisch, C., Pross, J., Fiebig, J., Petschick, R., Röhling, H.-G., Richoz, S., Rosenthal, Y., Falkowski, P.G., 2009. Floral changes across the Triassic/Jurassic boundary linked to flood basalt volcanism. Nat. Geosci. 2, 589–594. https://doi.org/10.1038/ngeo577.

van de Schootbrugge, B., van der Weijst, C.M.H., Hollaar, T.P., Vecoli, M., Strother, P.K., Kuhlmann, N., Thein, J., Visscher, H., van Konijnenburg-van Cittert, H., Schobben, M.A.N., Sluijs, A., Lindström, S., 2020. Catastrophic soil loss associated with end-Triassic deforestation. Earth-Sci. Rev. 210, 103332. https://doi.org/10.1016/j.earscirev.2020.103332.

Villar, H.J., Püttmann, W., Wolf, M., 1988. Organic geochemistry and petrography of Tertiary coals and carbonaceous shales from Argentina. Org. Geochem. 13, 1011–1021. https://doi.org/10.1016/0146-6380(88)90283-5.

Wignall, P.B., Atkinson, J.W., 2020. A two-phase end-Triassic mass extinction. Earth-Sci. Rev. 208, 103282. https://doi.org/10.1016/j.earscirev.2020.103282.

Wignall, P.B., Bond, D.P.G., 2008. The end-Triassic and Early Jurassic mass extinction records in the British Isles. Proc. Geol. Assoc. 119, 73–84. https://doi.org/10.1016/S0016-7878(08)80259-3.

Williford, K.H., Grice, K., Holman, A., McElwain, J.C., 2014. An organic record of terrestrial ecosystem collapse and recovery at the Triassic–Jurassic boundary in East Greenland. Geochim. Cosmochim. Acta 127, 251–263. https://doi.org/10.1016/j.gca.2013.11.033.

Wotzlaw, J.F., Guex, J., Bartolini, A., Gallet, Y., Krystyn, L., McRoberts, C.A., Taylor, D., Schoene, B., Schaltegger, U., 2014. Towards accurate numerical calibration of the late Triassic: highprecision U-Pb geochronology constraints on the duration of the Rhaetian. Geology 42, 571–574. https://doi.org/10.1130/G35612.1.

Yunker, M.B., Macdonald, R.W., Vingarzan, R., Mitchell, R.H., Goyette, D., Sylvestre, S., 2002. PAHs in the Fraser River basin: a critical appraisal of PAH ratios as indicators of PAH source and composition. Org. Geochem. 33, 489–515. https://doi.org/10.1016/S0146-6380(02)00002-5.

Zhang, X., Lv, P., Fang, L., Yang, H., Deng, S., Lu, Y., Fang, Y., Zhang, X., Huang, R., Liang, J., Shi, S., 2020. Widefire records across the Triassic-Jurassic boundary in the southern margin of the Junggar Basin and global correlations. Acta Sedimentol. Sin. https://doi.org/10.14027/j.issn.1000-0550.2020.103.